Article

A Metal-Free All-Carbon Nanohybrid for Ultra-Sensitive Photoelectrochemical Immunosensing of alpha-Fetoprotein

Qing Zhou, Huaijia Xue, Yuye Zhang, Yanqin Lv, Hongguang Li, Songqin Liu, Yanfei Shen, and Yuanjian Zhang

ACS Sens., **Just Accepted Manuscript** • DOI: 10.1021/acssensors.8b00307 • Publication Date (Web): 04 Jul 2018

A Metal-Free All-Carbon Nanohybrid for Ultra-Sensitive Photoelectrochemical Immunosensing of alpha-Fetoprotein

Qing Zhou,[a] Huaijia Xue,[a] Yuye Zhang,[a] Yanqin Lv,[a] Hongguang Li,[b] Songqin Liu,[a] Yanfei Shen,*[a] and Yuanjian Zhang*[a]

[a] School of Chemistry and Chemical Engineering, Medical School, Southeast University, Nanjing 211189, China, Email: Yanfei.Shen@seu.edu.cn, Yuanjian.Zhang@seu.edu.cn

[b] State Key Laboratory of Solid Lubrication & Laboratory of Clean Energy Chemistry and Materials, Lanzhou Institute of Chemical Physics, Chinese Academy of Sciences, Lanzhou, 730000, China

Abstract

C_{60} can accept up to six electrons reversibly and show exceptional light absorption over the entire UV-vis spectrum, making it a potential photoactive probe for photoelectrochemical (PEC) bioassay. However, few successful works have been reported to apply fullerenes in PEC biosensing, partially because of the low electronic conductivity and poor interfacial interactions with targeted biomolecules. Herein, we report the addressing of these two obstacles by coupling high conductive graphite flake (Gr), graphene oxide (GO) with sufficient oxygen-containing functional groups, and an alkylated C_{60} (AC_{60}) into a metal-free all-carbon nanohybrid (AC_{60}-Gr-GO) via harnessing delicate non-covalent interactions among them through a facile mechanical grinding. It was revealed that the as-obtained AC_{60}-Gr-GO nanohybrid not only showed conspicuous enhancement of photocurrent up to 35 times but also offered rich anchors for bioconjugation. Taking detecting Alpha-Fetoprotein as an example, the AC_{60}-Gr-GO based PEC immunosensor demonstrated a board linear detection range (1 $pg \cdot mL^{-1}$ ~ 100 $ng \cdot mL^{-1}$) and an detection limit as low as 0.54 $pg \cdot mL^{-1}$, superior/competitive to PEC immunosensors for AFP in previous reports. By a proper reinforcement in conductivity and bio-interface engineering, this work may provide a new way to pave fullerenes as photoactive materials in more general PEC biosensing.

Keywords

Fullerene, Conductivity reinforcement, Bio-interface engineering, Alpha-Fetoprotein, Photoelectrochemical biosensor

Photoelectrochemical (PEC) bioassay has drawn many attentions recently since it not only coupled the well-known merits of optical and electrochemical methods, but also has particular features such as high signal-to-noise ratio due to the complete isolation of the excitation and output signals.[1-6] Recently, many investigations have been undertaken to explorenew photoactive materials because a high efficient photoelectric conversion efficiency is a key to improve the analytical performances in PEC bioassay.[7-13] To date, several pioneering PEC biosensors have been constructed utilizing metal-containing semiconductors such as TiO_2, ZnO, WO_3, CdTe, and CdS nanoparticles or quantum dots (QDs),[14-19] which have exhibited excellent photoelectrochemical properties. Nevertheless, several improvements or concerns still need to be addressed before they enter the practical clinic applications, which include lowering environmental toxicity, improving biocompatibility, and enhancing the utilization of visible light.[20-23] Therefore, the development of photoactive materials for practical PEC biosensing is still in infancy.

Fullerenes, such as C_{60}, have attracted enormous interests both theoretically and experimentally due to their unique physiochemical properties.[24-31] Concretely, C_{60} can be reversibly reduced by accepting up to six electrons and exhibited a wide absorption in the whole UV-vis range, making it an attractive photoactive probe in constructing PEC biosensors.[32-34] However, few works have been reported for the applications of fullerenes in the research areas of PEC biosensing, partially due to the low electronic conductivity and poor interfacial interactions with biomolecules.[35-37] In principle, prospective properties could be achieved by a rational modification of fullerene into potential derivatives. In our previous work, we showed that the solubility of fullerene in organic solvents could be immensely enhanced by modifying fullerene with three long alkyl chain via a Prato reaction, and the photoelectric conversion efficiency of

alkylated fullerene C_{60} (AC_{60}) could be greatly improved by assembling with graphene due to the high affinity of long alkyl chain towards the graphene.[30]

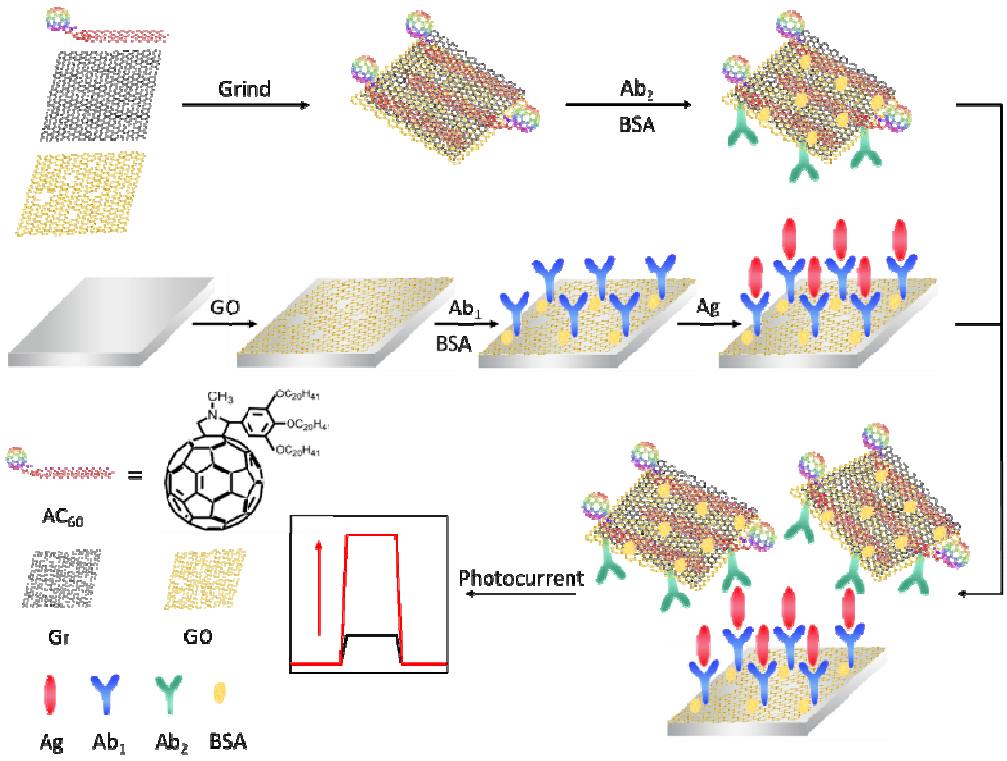

Figure 1. Scheme of general processes for assembling of AC_{60}-Gr-GO and construction of photoelectrochemcial AFP immunosensor.

To address the challenge of PEC biosensing application of fullerenes, herein, we report the coupling of AC_{60} with graphite flake (Gr) and graphene oxide (GO) into a metal-free all carbon nanohybrid (AC_{60}-Gr-GO) by a simple wet grinding method, thanks to delicate non-covalent interactions among them. As electron collector and transporter, the Gr in the assembly accelerated the charge-transfer and enhanced the photoelectric conversion efficiency of AC_{60} up to 35 times. Simultaneously, due to abundant carboxyl groups active sites, GO in the AC_{60}-Gr-GO nanohybrid guaranteed sufficient aqueous dispersity and a friendly anchors for facile bioconjugation. As an example, the AC_{60}-Gr-GO based PEC immunosensor (Figure 1) had a broad dynamic detection range from 1 pg·mL^{-1} to 100 ng·mL^{-1} and an detection limit of as low as

0.54 pg·mL^{-1} in sensing Alpha-Fetoprotein (AFP), which were superior/competitive to PEC immunosensors for AFP in previous reports.[38-43]

Experimental Section

Materials and Reagents

Alkylated-C_{60}, i.e., 3,4,5-Tris(eicosyloxy) phenyl substituted N-methyl-fulleropyrrolidine[60] (AC_{60}, Figure 1), was prepared by following the previous work.[44] Graphite flake (natural, -325 mesh, 99.8%) was obtained from Alfa Aesar Chemical Co. Ltd (Tianjin, China). Graphene oxide (GO) was homemade by a modified Hummers' method using the graphite flake as the precursor.[45] Alpha-Fetoprotein (AFP), Cardiac troponin I (cTnI), Mesothelin (MSLN), Tumor necrosis factor-α (TNF-α) and the antibody Ab_1 and Ab_2 were supplied by Beijing Key-Biotech Co. Ltd. 1-ethyl-3-(3-dimethylaminopropyl) carbodiimide (EDC) and N-hydroxysuccinimide (NHS) were offered by Sigma-Aldrich (Shanghai, China). Bovine serum albumin (BSA) and PBS solution was obtained from Sunshine Biotechnology Co. Ltd. (Nanjing, China) and Sangon Biotech (Shanghai, China), respectively. Ascorbic acid (AA), potassium ferricyanide, potassium ferrocyanide, acetone, tetrahydrofuran, and ethanol were supplied by Sinopharm Chemical Reagent Co. Ltd (China). Indium tin oxides (ITO, 6.2-6.8 Ω/sq) was purchased from Zhuhai Kaivo Optoelectronic Technology Co., Ltd (China). Ultrapure water (18.2 MΩ·cm) was used in the whole study from a Smart2Pure™water purification system (Thermo Fisher, USA).

Synthesis of AC_{60}-GO-Gr and further conjugation with Ab_2

The AC_{60}-Gr-GO nanohybrid was synthesized by a mechanical mixing of AC_{60}, Gr, and GO with a mass ratio of 1:0.1:1 (1 mg, 0.1 mg, 1 mg), and subsequent

sonication in 10 mL of 10 mM PBS for 2 h. After that, the supernatant was separated by using a centrifugation (800×g, 30 min). As control, Gr-GO nanohybrid that consisted of GO and graphite flake and AC_{60}-GO nanohybrid were individually prepared by similar procedures. For conjugation with Ab_2, 2 mL of the as-prepared AC_{60}-GO-Gr suspension was added into 200 μL of freshly prepared PBS solution (10 mM) containing EDC (100 mM) and NHS (50 mM). After that, the mixture was agitated using a ultrasonicator at room temperature under darkness for 30 min. Then, 60 μL of label antibody (Ab_2, 100 $\mu g \cdot mL^{-1}$) in PBS was further added into the reaction system, and the mixture was stirred at 4 ^oC for 12 h. At last, 20 mg of BSA was added with additional stirring for 1 h at 37 ^oC. The as-obtained $Ab_2@AC_{60}$-Gr-GO was kept at 4 ^oC and protected from light before use.

Preparation of various carbon assemblies photoelectrode

To examine the PEC behaviors of various carbon assemblies, various carbon assemblies-modified photoelectrodes were prepared. Briefly, prior to surface modification, the ITO glass was successively washed by using acetone, alcohol, and ultrapure water for 15 min, and blow-dried by using high pure nitrogen gas. Afterwards, various carbon assemblies-modified photoelectrodes were prepared by casting 10 μL dispersion of AC_{60}-Gr-GO, Gr-GO, AC_{60}-GO and AC_{60} onto the ITO surface (0.16 cm^2), respectively, and followed by drying in air.

Fabrication of photoelectrochemical immunosensor

Generally, 10 μL of the as-obtained GO dispersion (0.01 $mg \cdot mL^{-1}$) was drop casted onto the ITO electrode (0.16 cm^2) and dried in air (see the detailed optimization of GO/ITO thickness in Supporting Information). Afterwards, 10 μL of activation solution (10 mM, pH 6.0) consisted of EDC (100 mM) and NHS (50 mM) in PBS was drop-casted onto GO/ITO and kept for 2 h. After that, the un-reacted

activation agents on ITO was washed away using PBS solution. Then, 10 μL of capture antibody (Ab_1, 10 μg·mL^{-1}) in 10 mM PBS was added onto the ITO electrode and kept at 4 ^{o}C for another 12 h. After rinsing with PBS, the Ab_1 modified ITO was blocked by using BSA (1% w/v in 10 mM PBS) for 0.5 h at 37 ^{o}C. After removing excessive BSA by washing. The modified electrode was further reacted with AFP at 37 ^{o}C for 2 h. At last, 10 μL of Ab_2@ AC_{60}-Gr-GO dispersion was casted on the above-modified ITO electrode and kept at 37 ^{o}C for 2 h. The AFP immunosensor was thus prepared with sufficient rinsing using PBS.

Detection of AFP in serum

The serum collected from healthy people were diluted for 100 folds with 10 mM PBS. Then, the serum samples were spiked with the targeted AFP into 0.1, 0.5, 1, and 5 ng·mL^{-1}, respectively. The spiked serum samples were analyzed by the developed PEC immunosensor in this work. For each sample, three replicates were independently measured. The concentration of the spiked sample was calculated according to the calibration curve.

Apparatus

Cyclic voltammetry (CV), electrochemical impedance spectroscopy (EIS) and photoelectrochemical studies were undertaken on a Reference 600 potentiostat/galvanostat/ZRA (Gamry, USA). Three-electrode system was used, consisting of the modified ITO as the working electrode, an Ag/AgCl (saturated KCl) as the reference electrode, and platinum wire as the counter electrode. The transmission electron microscopy (TEM) images were measured with a field emission electron microscopy (JEM-2100f, JEOL, Japan). The scanning electron microscopy (SEM) images were collected using a tabletop scanning electron microscope (Phenom ProX, Netherlands). UV−vis absorption spectra were measured using an UV−vis

spectrophotometer (Cary100, Agilent, Singapore). Powder X-ray diffraction (XRD) was performed on an X-ray diffractometer (Ultima IV, Rigaku, Japan). Raman spectra (E_x = 532 nm) were measured using a micro Raman spectrophotometer (DXR-laser, Thermo, USA). The electrolyte for photoelectrochemical studies consisted of PBS (10 mM, pH = 6) and additional AA (0.1 M) as the sacrificial agent. [46] A Xe lamp (150 W, Beijing NBeT Co., Ltd.) was utilized as the source of visible light. The photocurrents were collected at a fixed biased potential (-0.2 V, see more discussion in Figure S4).

Results and Discussion

Structures of AC_{60}-Gr-GO nanohybrid

In order to enhance the PEC performance and provide more active sites for further conjugation with biomolecules for AC_{60}, a AC_{60}-Gr-GO nanohybrid was prepared via a noncovalent interaction.[47-48] It was because the graphite flake could enhance the electric conductivity of AC_{60}-Gr-GO, while the GO in AC_{60}-Gr-GO provided sufficient hydrophilic oxygen-containing groups such as -COOH and -OH, which were favor of dispersion in aqueous solution and the conjugation with biomolecules to AC_{60}-Gr-GO nanohybrid. The formation of AC_{60}-Gr-GO nanohybrid was firstly investigated by SEM (Figure 2a) and TEM (Figure 2b) images. It was observed that both of them demonstrated wavy sheets, typical morphology of graphene-derivative materials. Notably, TEM image (Figure 2c) of AC_{60}-Gr-GO revealed a uniform distribution of sphere like nanoclusters, most presumably of AC_{60}, on the surface of Gr-GO nanosheet. High-resolution TEM (HRTEM) image in Figure 2c inset further demonstrate the lattice fringes of these nanocluster, indicative of a crystallinity AC_{60}, which was favor of suppressing unwanted exciton recombination in photoelectric conversion.[49]

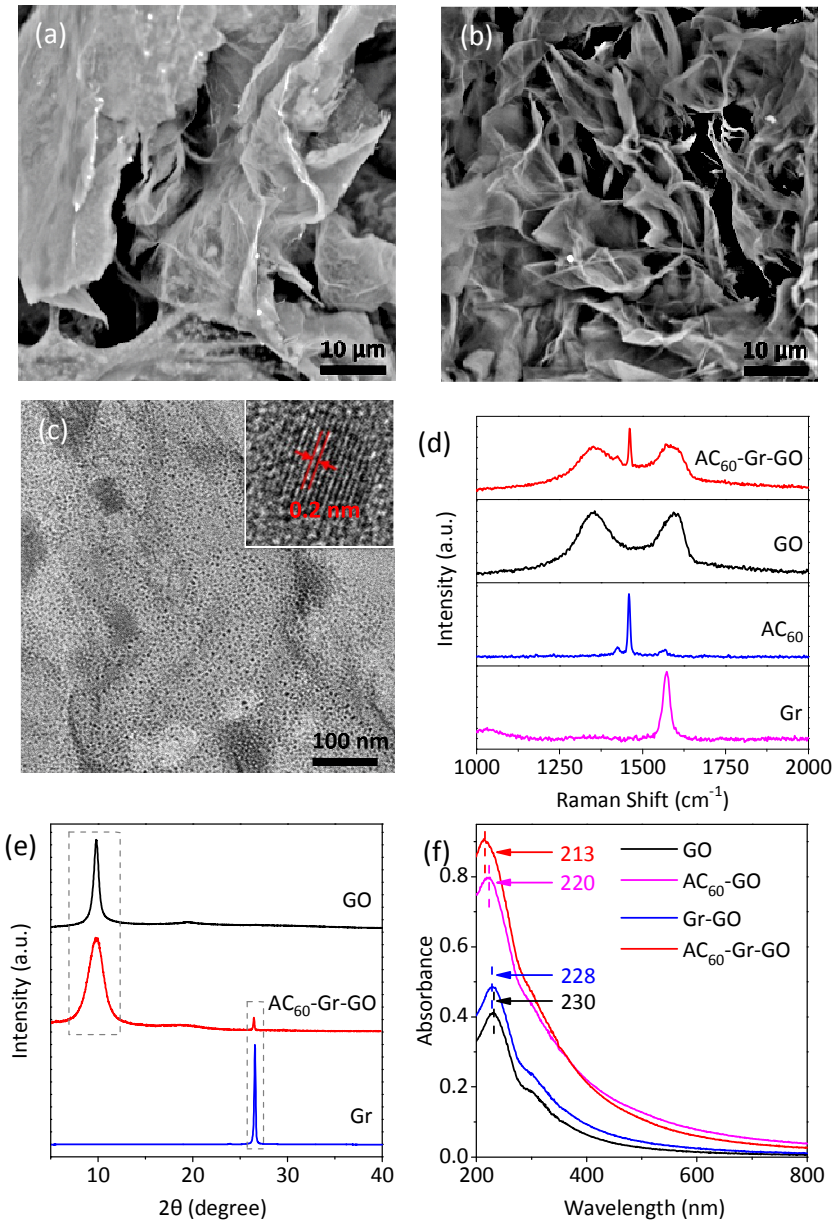

Figure 2. SEM images of AC_{60}-Gr-GO (a) and Gr-GO (b). TEM image of AC_{60}-Gr-GO (c). Inset shows the HRTEM image of the AC_{60} in AC_{60}-Gr-GO. Raman spectra of AC_{60}-Gr-GO, GO, AC_{60} and Gr (d). (e) XRD spectra of AC_{60}-Gr-GO, Gr and GO. UV-vis spectra of AC_{60}-Gr-GO, Gr-GO, AC_{60}-GO and GO (f).

The successful synthesis of AC_{60}-Gr-GO was further verified by Raman spectroscopy. Figure 2d showed the Raman spectra of AC_{60}-Gr-GO, AC_{60}, Gr and GO with 532 nm laser excitation. For both GO and AC_{60}-Gr-GO, the D/G bands were

evidently observed at ca. 1350 cm^{-1} and 1590 cm^{-1}, respectively. In contrast, the spectrum of Gr only showed a strong peak at ca. 1590 cm^{-1} due to the perfect graphitic structure. Interestingly, compared with that of GO, the G/D ratio of AC_{60}-Gr-GO became larger, confirming the existence of Gr in the AC_{60}-Gr-GO. Furthermore, the Raman peak of C_{60} was clearly remained in AC_{60}-Gr-GO, suggesting the successful synthesis of AC_{60}-Gr-GO nanohybrid and the preservation of basic structure of AC_{60} after the assembly. Complementarily, the X-ray diffraction (XRD) showed that the AC_{60}-Gr-GO retained the identical predominant 002 diffraction of GO and Gr (Figure 2e), suggesting the existence of GO and Gr in AC_{60}-Gr-GO. Because AC_{60} is insoluble in aqueous solution (see the UV-vis absorption spectrum of AC_{60} in Figure S1), the electronic interactions among these carbon nanohybrids in aqueous solution were investigated using the typical absorption of GO in the UV region as the indicator. Notably, the maximum absorption of GO at 230 nm, which was commonly assigned to the π-π^* transition of aromatic C=C bond, showed blue shift in Gr-GO (228 nm), AC_{60}-GO (220 nm) and AC_{60}-Gr-GO (213 nm), which suggested an electron transfer among GO and AC_{60}, and graphite sheets.[50-53] Such electron-communication could be ascribed to the π-π non-covalent interactions among them. In addition, the UV-vis spectra (Figure 2f) showed the absorbance of AC_{60}-Gr-GO was much higher than that of Gr-GO, confirming the wide light absorption in the whole UV-vis range due to AC_{60}.[30] Therefore, AC_{60}-Gr-GO nanohybrid was successfully prepared.

Photoelectrochemical behavior of AC_{60}-Gr-GO nanohybrid

To evaluate the PEC activities of AC_{60}-Gr-GO nanohybrid, the photocurrent generation was measured by a standard photoelectrochemical cell configuration under chopped light irradiation. As shown in Figure 3a, photocurrents of all electrodes were

prompt, steady and reproducible under the chopped light. Moreover, the photocurrent of ITO/AC_{60}-Gr-GO was up tp 5.3 μA, already as high as 35-times that of the AC_{60} alone (Figure 3a). In addition, the photocurrent of ITO/AC_{60}-GO was about 2.5 μA, which was less than half of that of ITO/AC_{60}-Gr-GO, probably because of the excellent conductivity of Gr. To verify this assumption, as shown in Figure 3b, the cyclic voltammograms (CV) at ITO/AC_{60}-Gr-GO and ITO/AC_{60}-GO both showed a pair of well-defined reduction and oxidation waves of $[Fe(CN)_6]^{3-}$. Notably, the CV at ITO/AC_{60}-Gr-GO displayed a higher peak current and less peak potential difference than that at ITO/AC_{60}-GO, suggesting that Gr significantly improved the conductivity of the AC_{60}-Gr-GO.[54] Furthermore, the AC_{60}-Gr-GO showed higher electrochemical active surface area (Figure S2a-c) and enhanced conductivity (Figure S2d) than AC_{60}-GO.

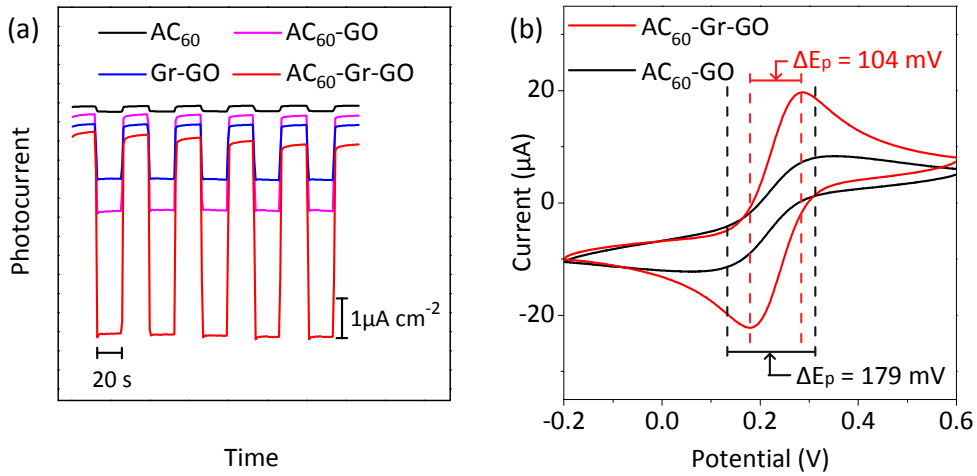

Figure 3. (a) Photocurrent of AC_{60}-GO-Gr, GO-Gr, AC_{60}-GO and AC_{60} modified ITO. (b) Cyclic voltammograms of AC_{60}-Gr-GO and AC_{60}-GO modified ITO in 10 mM PBS solution containing 2 mM $K_3[Fe(CN)_6]$. Scan rate: 100 $mV \cdot s^{-1}$.

Construction of photoelectrochemical immunosensor

The step-by-step assembling process for the immunosensor configuration was

monitored by CV and EIS measurements. As indicated in Figure 4a, CV of 2 mM $K_3[Fe(CN)_6]$ at the naked ITO exhibits two well-defined reduction and oxidation waves with a small anodic and cathodic peak potential difference (ΔE_p, <80 mV), suggsting highly reversible electrochemical reactions at bare ITO. After GO, Ab_1, BSA and AFP were successively attached on ITO, the peak currents decreased gradually, suggesting a inhibited electron transfer of $K_3[Fe(CN)_6]$ at ITO due to the poor conductivity of the biomolecules. Notably, the peak currents conversely increased upon the anchor of Ab_2@ AC_{60}-Gr-GO in the last assembling step, which most presumably due to the good conductivity Gr-GO in the nanohybrid.[55] The variation of charge transfer resistance (denoted as R_{ct}) at the modified ITO during the immunosensor construction was evaluated by EIS (Figure 4b). The EIS spectrum was recorded from 0.1 to 10^5 Hz at 0.22 V in PBS (10 mM, pH 7.4) containing 5 mM $[Fe(CN)_6]^{3-/4-}$. It was observed that the diameter of the semicircle on the Nyquist plots, roughly associated with R_{ct} at the electrode/solution interface, increased gradually with the successive assembling GO (53 Ω), Ab_1 (98 Ω), and AFP (213 Ω) on ITO compared with that of bare ITO (41 Ω), and then decreased with the further binding of Ab_2@ AC_{60}- Gr-GO (164 Ω). The change trend of R_{ct} was in agree with the CV results. Thus, both CV and EIS measurement suggested the successful construction of PEC immunosensor.

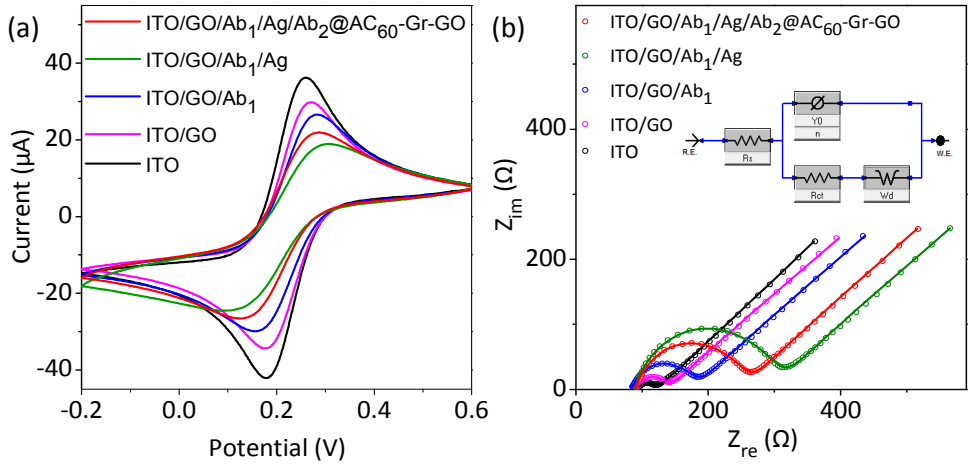

Figure 4. (a) Cyclic voltammograms of AC_{60}-Gr-GO based photoelectrochemical immunosensor after each step of assembly. Electrolytes: 2 mM $K_3[Fe(CN)_6]$ in 10 mM PBS solution. Scan rate: 100 $mV \cdot s^{-1}$. (b) Nyquist plots (scatters) and simulation (lines) of AC_{60}-Gr-GO based photoelectrochemical immunosensor after each step of assembly. Inset: the equivalent circuit. Electrolytes: 5 mM $[Fe(CN)_6]^{3-/4-}$ in 10 mM PBS solution.

Biosensing performance of the AC_{60}-Gr-GO based photoelectrochemical immunosensor

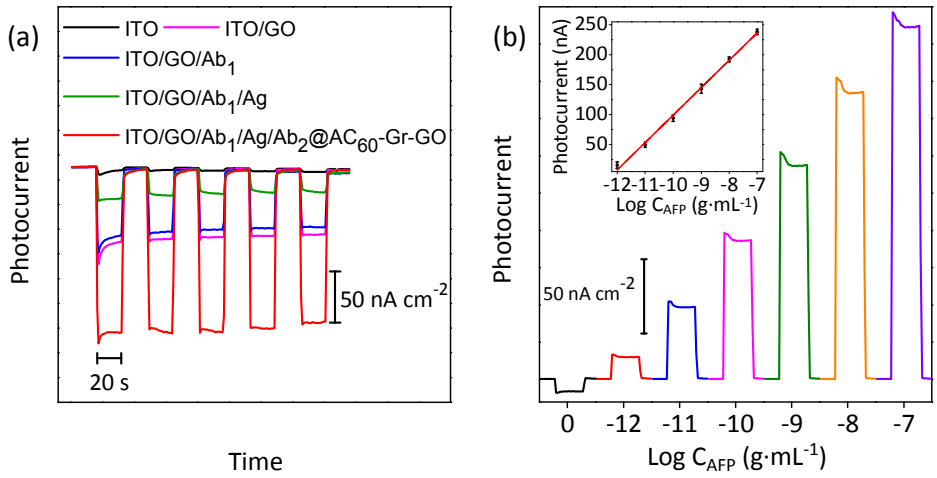

Figure 5. (a) Photocurrent of the modified ITO after each assembling step in immunosensor fabrication. (b) Photocurrent of the as-prepared PEC immunosensor in the presence of AFP with different concentrations. Inset shows the calibration plot.

It was supposed that the Ab_2@ AC_{60}-Gr-GO would be captured via a stoichiometric immunoreaction. It was observed that the photocurrent reduced gradually with the successive assembling Ab_1, and Ag (Figure 5a), presumably due to the steric resistance of these poor conductive biomolecules. However, an obvious increase appeared after the immunoreaction of Ab_2@AC_{60}-Gr-GO with AFP, which could be ascribed to the excellent photoelectric activity of AC_{60}-Gr-GO nanohybrid. Thus, the Ab_2@ AC_{60}-Gr-GO was applicable as an effective probe in sensing AFP based on the increase of photocurrent after the assembly of Ab_2@ AC_{60}-Gr-GO. As shown in Figure 5b, the photocurrent increased gradually with the concentration of AFP increase. The calibration curve in Figure 5b inset demonstrated that the photocurrent was linear to the logarithm values of AFP concentrations ranging from 1 $pg{\cdot}mL^{-1}$ to 100 $ng{\cdot}mL^{-1}$. Using the linear fitting ($r = 0.9970$), the relationship of ΔI and C_{AFP} could be described as $\Delta I = 557.4442 + 45.8172 \log C_{AFP}$ ($g{\cdot}mL^{-1}$). The limit of detection (LOD, $3\sigma/S$) was calculated to be 0.54 $pg{\cdot}mL^{-1}$ (according to. Compared with the well-developed PEC immunosensors utilizing metal-containing photoactive materials such as CdSe and CdS QDs, the sensing performances of the current PEC immunoassay were superior/competitive to those in previous reports as summarized in Table 1. Therefore, the AC_{60}-Gr-GO nanohybrid would be a very promising PEC probefor immunoassay.

Table 1. Comparison of AFP immunoassay performances by using different PEC probes.

Photoactive material	Linear range ($ng{\cdot}mL^{-1}$)	LOD ($pg{\cdot}mL^{-1}$)	Reproducibility (%)	References
CuO NPs	0.05-500	38	-	38
Au NPs@ZnO micro-flowers	0.005-50	0.56	-	39

CdS QDs	0.1-500	10	5.4	40
CdS QDs	0.0001-160	0.03	3.6	41
CdSe QDs	0.001-1000	0.31	3.8	42
CdS QDs@ mesoporous TiO_2	0.05-20	20	-	43
AC_{60}-Gr-GO	0.001-100	0.54	2.3	This work

Specificity, Reproducibility, Stability, and Reliability

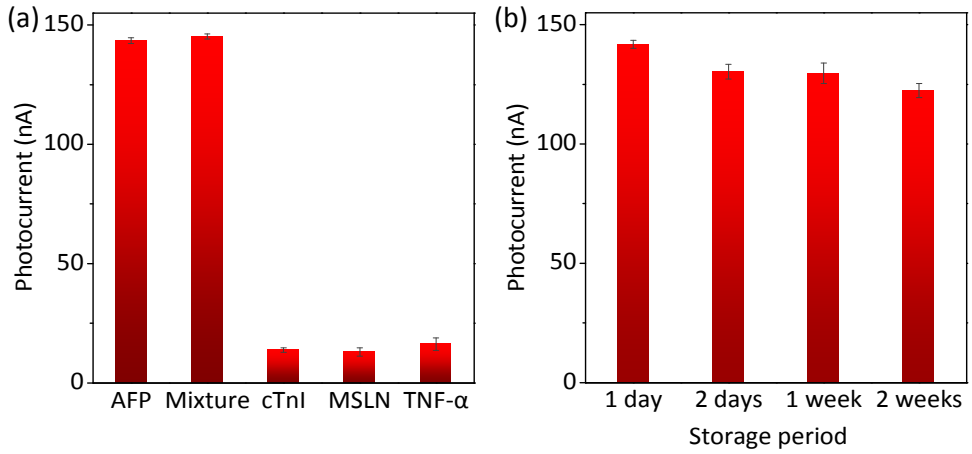

Figure 6. (a) Photocurrent of the immunosensor for 1 ng·mL^{-1} AFP, cTnI, MSLN, TNF-α, or the mixture of them in PBS. (b) Stability evaluation of the proposed PEC immunosensor for detecting 1 ng·mL^{-1} AFP.

To evaluate the specificity of the proposed immunosensor, the modified electrodes (ITO/GO/Ab_1/BSA) were incubated with AFP, Cardiac troponin I (cTnI), Mesothelin (MSLN), Tumor necrosis factor-α (TNF-α), and the mixture of them. As shown in Figure 6a, the photocurrents of the immunosensor for cTnI, MSLN and TNF-α were much lower than that for AFP and the mixture. It suggested that these potential interfering biomolecules had negligible influence for the highly selective detection of AFP. The reproducibility of the proposed PEC immunosensor was also undertaken. It was revealed that by six independent experiments, the proposed

immunosensors exhibited excellent reproducibility with a minor relative standard deviation (RSD, 2.31%). Moreover, the stability of the proposed immunosensor was also examined (Figure 6b). By storing the immunosensor (ITO/GO/Ab_1/BSA/AFP/Ab_2@AC_{60}-Gr-GO) for 1 ng·mL^{-1} AFP in PBS (10 mM, pH 7.4) at 4 ^{o}C under darkness, 98.84% and 90.85% of the initial signal was maintained in 1 and 2 days, respectively. Even after 1 and 2 weeks, the immunosensor still retained 90.36% and 85.32% of the initial signal, respectively. It suggested that the stability of the AC_{60}-Gr-GO-based immunosensor was high.

Table 2. Recovery experiments for sensing AFP in the spiked serum samples from human.

Human serum sample no.	Spiked AFP (ng·mL^{-1})	Found	Recovery (%)	RSD (%)
1	0	0.1479	-	3.08
2	0.1	0.2501	102.20	2.36
3	0.5	0.6607	102.56	3.32
4	1	1.1220	97.41	1.76
5	5	5.1381	99.80	1.42

To evaluate the reliability of the AC_{60}-Gr-GO-based PEC immunosensor, four spiked human serum samples collected from healthy volunteers containing 0.1, 0.5, 1, or 5 ng·mL^{-1} AFP were checked. For each sample, the test was independently undertaken for three times. The concentration of AFP was calculated according to the calibration curve in Figure 5b inset. As listed in Table 2, the recoveries of all spiked samples were between 97.40% and 102.56%, and the relative standard deviation (RSD) was less than 3.32%. Such satisfied recoveries and RSD suggested the AC_{60}-Gr-GO-based PEC immunosensor was promising for sensing AFP in clinical examination.

Conclusion

In this work, a metal-free all carbon nanohybrid, i.e. AC_{60}-Gr-GO, via harnessing delicate noncovalent interactions was prepared using a facile wet grinding method, and was explored as a emerging PEC probe in an immunosensor for detecting AFP. The coupling of Gr and GO to AC_{60} not only showed conspicuous enhancement of photocurrent up to 35 times due to the reinforcement in conductivity but also provided abundant binding sites for the conjugation of biomolecules. As an example, the AC_{60}-Gr-GO based AFP PEC immunosensor showed superior/competitive performances with respect to AFP biosensors using other photoactive materials including metal-containing QDs in previous reports. It also had a broad linear detection range (1 $pg \cdot mL^{-1}$ ~ 100 $ng \cdot mL^{-1}$) and a detection limit as low as 0.54 $pg \cdot mL^{-1}$. This work highlight the great potential of fullerene-based nanohybrid as highly sensitive PEC probe in biosensing for early disease diagnosis.

Supporting Information

The Supporting Information is available free of charge on the ACS Publications website at DOI: 10.1021/xxxxxxx.

UV-vis absorption spectrum of AC_{60}, EASA evaluation and EIS of AC_{60}-Gr-GO, GO thickness optimization, I-V curve of AC_{60}-Gr-GO under the chopped light, and more discussion (PDF)

Acknowledgements

This work was supported by the National Natural Science Foundation of China (21675022, 21775018), the Natural Science Foundation of Jiangsu Province (BK20160028, BK20170084), the Open Funds of the State Key Laboratory of

Electroanalytical Chemistry (SKLEAC201703) and the Fundamental Research Funds for the Central Universities.

References

(1) Haddour, N.; Chauvin, J.; Gondran, C.; Cosnier, S. Photoelectrochemical immunosensor for label-free detection and quantification of anti-cholera toxin antibody. *J. Am. Chem. Soc.* **2006,** *128,* 9693-9698.

(2) Li, Z.; Su, C.; Wu, D.; Zhang, Z. Gold Nanoparticles Decorated Hematite Photoelectrode for Sensitive and Selective Photoelectrochemical Aptasensing of Lysozyme. *Anal. Chem.* **2018,** *90,* 961-967.

(3) Trashin, S.; Rahemi, V.; Ramji, K.; Neven, L.; Gorun, S. M.; De Wael, K. Singlet oxygen-based electrosensing by molecular photosensitizers. *Nat. Commun.* **2017,** *8,* 10.

(4) Willner, I.; Patolsky, F.; Wasserman, J. Photoelectrochemistry with controlled DNA-cross-linked CdS nanoparticle arrays. *Angew. Chem. Int. Edit.* **2001,** *40,* 1861-1864.

(5) Zhan, W. W.; Kuang, Q.; Zhou, J. Z.; Kong, X. J.; Xie, Z. X.; Zheng, L. S. Semiconductor@Metal-Organic Framework Core-Shell Heterostructures: A Case of ZnO@ZIF-8 Nanorods with Selective Photoelectrochemical Response. *J. Am. Chem. Soc.* **2013,** *135,* 1926-1933.

(6) Zhao, W. W.; Xu, J. J.; Chen, H. Y. Photoelectrochemical bioanalysis: the state of the art. *Chem. Soc. Rev.* **2015,** *44,* 729-741.

(7) Bellani, S.; Ghadirzadeh, A.; Meda, L.; Savoini, A.; Tacca, A.; Marra, G.; Meira, R.; Morgado, J.; Di Fonzo, F.; Antognazza, M. R. Hybrid Organic/Inorganic Nanostructures for Highly Sensitive Photoelectrochemical Detection of Dissolved Oxygen in Aqueous Media. *Adv. Funct. Mater.* **2015,** *25,* 4531-4538.

(8) Guo, L. M.; Li, Z.; Marcus, K.; Navarro, S.; Liang, K.; Zhou, L.; Mani, P. D.; Florczyk, S. J.; Coffey, K. R.; Orlovskaya, N.; Sohn, Y. H.; Yang, Y. Periodically Patterned Au-TiO2 Heterostructures for Photoelectrochemical Sensor. *ACS Sens.* **2017,** *2,* 621-625.

(9) Metzger, T. S.; Chandaluri, C. G.; Tel-Vered, R.; Shenhar, R.; Willner, I. Donor/Acceptor-Modified Electrodes for Photoelectrochemical and

Photobioelectrochemical Applications. *Adv. Funct. Mater.* **2016,** *26,* 7148-7155.

(10) Nallal, M.; Iyengar, G. A.; Pill-Lee, K. New Titanium Dioxide-Based Heterojunction Nanohybrid for Highly Selective Photoelectrochemical Electrochemical Dual-Mode Sensors. *ACS Appl. Mater. Interfaces* **2017,** *9,* 37166-37183.

(11) Tang, J.; Zhang, Y. Y.; Kong, B.; Wang, Y. C.; Da, P. M.; Li, J.; Elzatahry, A. A.; Zhao, D. Y.; Gong, X. G.; Zheng, G. F. Solar-Driven Photoelectrochemical Probing of Nanodot/Nanowire/Cell Interface. *Nano Lett.* **2014,** *14,* 2702-2708.

(12) Xu, J.; Shalom, M. Electrophoretic Deposition of Carbon Nitride Layers for Photoelectrochemical Applications. *ACS Appl. Mater. Interfaces* **2016,** *8,* 13058-13063.

(13) Wang, L.; Han, D.; Ni, S.; Ma, W.; Wang, W.; Niu, L. Photoelectrochemical device based on Mo-doped BiVO4 enables smart analysis of the global antioxidant capacity in food. *Chem Sci* **2015,** *6,* 6632-6638.

(14) Li, W.; Sheng, P. T.; Cai, J.; Feng, H. Y.; Cai, Q. Y. Highly sensitive and selective photoelectrochemical biosensor platform for polybrominated diphenyl ether detection using the quantum dots sensitized three-dimensional, macroporous ZnO nanosheet photoelectrode. *Biosens. Bioelectron.* **2014,** *61,* 209-214.

(15) Ma, W.; Wang, L.; Zhang, N.; Han, D.; Dong, X.; Niu, L. Biomolecule-Free, Selective Detection of o-Diphenol and Its Derivatives with WS2/TiO2-Based Photoelectrochemical Platform. *Anal. Chem.* **2015,** *87,* 4844-4850.

(16) Pang, X. H.; Bian, H. J.; Su, M. H.; Ren, Y. Y.; Qi, J. N.; Ma, H. M.; Wu, D.; Hu, L. H.; Du, B.; Wei, Q. Photoelectrochemical Cytosensing of RAW264.7 Macrophage Cells Based on a TiO2 Nanoneedls@MoO3 Array. *Anal. Chem.* **2017,** *89,* 7950-7957.

(17) Tabrizi, M. A.; Shamsipur, M.; Saber, R.; Sarkar, S.; Ebrahimi, V. A high sensitive visible light-driven photoelectrochemical aptasensor for shrimp allergen tropomyosin detection using graphitic carbon nitride-TiO2 nanocomposite. *Biosens. Bioelectron.* **2017,** *98,* 113-118.

(18) Wang, X. P.; Xu, R.; Sun, X.; Wang, Y. G.; Ren, X.; Du, B.; Wu, D.; Wei, Q. Using reduced graphene oxide-Ca:CdSe nanocomposite to enhance photoelectrochemical activity of gold nanoparticles functionalized tungsten oxide for highly sensitive prostate specific antigen detection. *Biosens. Bioelectron.* **2017,** *96,* 239-245.

(19) Yang, Y.; Hu, W. H. Bifunctional polydopamine thin film coated zinc oxide

nanorods for label-free photoelectrochemical immunoassay. *Talanta* **2017,** *166,* 141-147.

(20) Li, X.; Zhu, L. S.; Zhou, Y. L.; Yin, H.; Ai, S. Y. Enhanced Photoelectrochemical Method for Sensitive Detection of Protein Kinase A Activity Using TiO2/g-C3N4, PAMAM Dendrimer, and Alkaline Phosphatase. *Anal. Chem.* **2017,** *89,* 2369-2376.

(21) Qiu, T. A.; Meyer, B. M.; Christenson, K. G.; Klaper, R. D.; Haynes, C. L. A mechanistic study of TiO2 nanoparticle toxicity on Shewanella oneidensis MR-1 with UV-containing simulated solar irradiation: Bacterial growth, riboflavin secretion, and gene expression. *Chemosphere* **2017,** *168,* 1158-1168.

(22) Wang, H. Y.; Zhang, Q. H.; Yin, H. S.; Wang, M. H.; Jiang, W. J.; Ai, S. Y. Photoelectrochemical immunosensor for methylated RNA detection based on g-C3N4/CdS quantum dots heterojunction and Phos-tag-biotin. *Biosens. Bioelectron.* **2017,** *95,* 124-130.

(23) Wang, J.; Sun, J. J.; Hu, C. G.; Liu, Z. H.; Hu, S. S. Facile synthesis of flexible gold film electrodes for highly selective photoelectrochemical sensing of ascorbic acid. *J Electroanal Chem* **2015,** *759,* 2-7.

(24) Bai, L. J.; Chen, Y. H.; Bai, Y.; Chen, Y. J.; Zhou, J.; Huang, A. L. Fullerene-doped polyaniline as new redox nanoprobe and catalyst in electrochemical aptasensor for ultrasensitive detection of Mycobacterium tuberculosis MPT64 antigen in human serum. *Biomater* **2017,** *133,* 11-19.

(25) Giordani, S.; Colomer, J. F.; Cattaruzza, F.; Alfonsi, J.; Meneghetti, M.; Prato, M.; Bonifazi, D. Multifunctional hybrid materials composed of 60 fullerene-based functionalized-single-walled carbon nanotubes. *Carbon* **2009,** *47,* 578-588.

(26) Liu, Q. L.; Guan, M. R.; Xu, L.; Shu, C. Y.; Jin, C.; Zheng, J. P.; Fang, X. H.; Yang, Y. J.; Wang, C. R. Structural Effect and Mechanism of C70-Carboxyfullerenes as Efficient Sensitizers against Cancer Cells. *Small* **2012,** *8,* 2070-2077.

(27) Mojarad, N.; Tisserant, J. N.; Beyer, H.; Dong, H.; Reissner, P. A.; Fedoryshyn, Y.; Stemmer, A. Monitoring the transformation of aliphatic and fullerene molecules by high-energy electrons using surface-enhanced Raman spectroscopy. *Nanotechnology* **2017,** *28,* 9.

(28) Prasad, S. B.; Kumar, A.; Singh, R. Molecularly imprinted polymer-based electrochemical sensor using functionalized fullerene as a nanomediator for ultratrace analysis of primaquine. *Carbon* **2016,** *109,* 196-207.

(29) Praveen, V. K.; Ranjith, C.; Bandini, E.; Ajayaghosh, A.; Armaroli, N.

Oligo(phenylenevinylene) hybrids and self-assemblies: versatile materials for excitation energy transfer. *Chem. Soc. Rev.* **2014,** *43,* 4222-4242.

(30) Shen, Y.; Saeki, A.; Seki, S.; Lee, J.-O.; Aimi, J.; Nakanishi, T. Exfoliation of Graphene and Assembly Formation with Alkylated-C60: A Nanocarbon Hybrid towards Photo-Energy Conversion Electrode Devices. *Adv. Optical Mater.* **2015,** *3,* 925-930.

(31) Zhang, C.; He, J.; Zhang, Y.; Chen, J.; Zhao, Y.; Niu, Y.; Yu, C. Cerium dioxide-doped carboxyl fullerene as novel nanoprobe and catalyst in electrochemical biosensor for amperometric detection of the CYP2C19*2 allele in human serum. *Biosens. Bioelectron.* **2018,** *102,* 94-100.

(32) Afreen, S.; Muthoosamy, K.; Manickam, S.; Hashim, U. Functionalized fullerene (C(6)(0)) as a potential nanomediator in the fabrication of highly sensitive biosensors. *Biosens. Bioelectron.* **2015,** *63,* 354-364.

(33) Li, M. J.; Zheng, Y. N.; Liang, W. B.; Yuan, R.; Chai, Y. Q. Using p-type PbS Quantum Dots to Quench Photocurrent of Fullerene-Au NP@MoS2 Composite Structure for Ultrasensitive Photoelectrochemical Detection of ATP. *ACS Appl. Mater. Interfaces* **2017,** *9,* 42111-42120.

(34) Zhu, P. H.; Wang, P. P.; Kan, T. L.; Sun, G. Q.; Zhang, Y.; Yu, J. H. An enhanced photoelectrochemical immunosensing platform: Supramolecular donor-acceptor arrays by assembly of porphyrin and C-60. *Biosens. Bioelectron.* **2015,** *68,* 604-610.

(35) Han, J.; Zhuo, Y.; Chai, Y. Q.; Xiang, Y.; Yuan, R. New type of redox nanoprobe: C60-based nanomaterial and its application in electrochemical immunoassay for doping detection. *Anal. Chem.* **2015,** *87,* 1669-1675.

(36) Hu, C.; Zheng, J.; Su, X.; Wang, J.; Wu, W.; Hu, S. Ultrasensitive all-carbon photoelectrochemical bioprobes for zeptomole immunosensing of tumor markers by an inexpensive visible laser light. *Anal. Chem.* **2013,** *85,* 10612-10619.

(37) Li, M. J.; Zheng, Y. N.; Liang, W. B.; Yuan, Y. L.; Chai, Y. Q.; Yuan, R. An ultrasensitive "on-off-on" photoelectrochemical aptasensor based on signal amplification of a fullerene/CdTe quantum dots sensitized structure and efficient quenching by manganese porphyrin. *Chem. Commun.* **2016,** *52,* 8138-8141.

(38) Wen, G. M.; Ju, H. X. Ultrasensitive photoelectrochemical immunoassay through tag induced exciton trapping. *Talanta* **2015,** *134,* 496-500.

(39) Han, Z.; Luo, M.; Chen, L.; Chen, J.; Li, C. A photoelectrochemical immunosensor for detection of α-fetoprotein based on Au-ZnO flower-rod

heterostructures. *Appl. Surf. Sci.* **2017,** *402,* 429-435.

(40) Xu, R.; Jiang, Y.; Xia, L.; Zhang, T.; Xu, L.; Zhang, S.; Liu, D.; Song, H. A sensitive photoelectrochemical biosensor for AFP detection based on ZnO inverse opal electrodes with signal amplification of CdS-QDs. *Biosens. Bioelectron.* **2015,** *74,* 411-417.

(41) Dai, H.; Zhang, S.; Gong, L.; Li, Y.; Xu, G.; Lin, Y.; Hong, Z. The photoelectrochemical exploration of multifunctional TiO2 mesocrystals and its enzyme-assisted biosensing application. *Biosens. Bioelectron.* **2015,** *72,* 18-24.

(42) Chen, J.; Zhao, G. C. A novel signal-on photoelectrochemical immunosensor for detection of alpha-fetoprotein by in situ releasing electron donor. *Biosens. Bioelectron.* **2017,** *98,* 155-160.

(43) Yang, X.; Li, J.; Fu, J. A novel photoelectrochemical sensor for the detection of α-fetoprotein based on a mesoporous TiO2–CdS QD composite film. *Anal. Methods* **2015,** *7,* 1328-1332.

(44) Nakanishi, T.; Michinobu, T.; Yoshida, K.; Shirahata, N.; Ariga, K.; Moehwald, H.; Kurth, D. G. Nanocarbon superhydrophobic surfaces created from fullerene-based hierarchical supramolecular assemblies. *Adv. Mater.* **2008,** *20,* 443-446.

(45) Zhang, Y. J.; Fugane, K.; Mori, T.; Niu, L.; Ye, J. H. Wet chemical synthesis of nitrogen-doped graphene towards oxygen reduction electrocatalysts without high-temperateure pyrolysis. *J. Mater. Chem.* **2012,** *22,* 6575-6580.

(46) Mi, L.; Wang, P.; Yan, J.; Qian, J.; Lu, J.; Yu, J.; Wang, Y.; Liu, H.; Zhu, M.; Wan, Y.; Liu, S. A novel photoelectrochemical immunosensor by integration of nanobody and TiO(2) nanotubes for sensitive detection of serum cystatin C. *Anal. Chim. Acta.* **2016,** *902,* 107-114.

(47) Shen, Y. F.; Reparaz, J. S.; Wagner, M. R.; Hoffmann, A.; Thomsen, C.; Lee, J. O.; Heeg, S.; Hatting, B.; Reich, S.; Saeki, A.; Seki, S.; Yoshida, K.; Babu, S. S.; Mohwald, H.; Nakanishi, T. Assembly of carbon nanotubes and alkylated fullerenes: nanocarbon hybrid towards photovoltaic applications. *Chem. Sci.* **2011,** *2,* 2243-2250.

(48) Zhou, Q.; Li, G. H.; Zhang, Y. J.; Zhu, M.; Wan, Y. K.; Shen, Y. F. Highly Selective and Sensitive Electrochemical Immunoassay of Cry1C Using Nanobody and pi-pi Stacked Graphene Oxide/Thionine Assembly. *Anal. Chem.* **2016,** *88,* 9830-9836.

(49) Wang, J. H.; Shen, Y. F.; Li, Y.; Liu, S. Q.; Zhang, Y. J. Crystallinity Modulation of Layered Carbon Nitride for Enhanced Photocatalytic Activities. *Chem. Eur. J.* **2016,** *22,* 12449-12454.

(50) Naumov, A.; Grote, F.; Overgaard, M.; Roth, A.; Halbig, C. E.; Norgaard, K.; Guldi, D. M.; Eigler, S. Graphene Oxide: A One- versus Two-Component Material. *J. Am. Chem. Soc.* **2016,** *138,* 11445-11448.

(51) Liu, H.; Kuila, T.; Kim, N. H.; Ku, B.-C.; Lee, J. H. In situ synthesis of the reduced graphene oxide–polyethyleneimine composite and its gas barrier properties. *J. Mater. Chem. A* **2013,** *1,* 3739.

(52) Xu, L. Q.; Yang, W. J.; Neoh, K.-G.; Kang, E.-T.; Fu, G. D. Dopamine-Induced Reduction and Functionalization of Graphene Oxide Nanosheets. *Macromolecules* **2010,** *43,* 8336-8339.

(53) Robinson, J. T.; Tabakman, S. M.; Liang, Y.; Wang, H.; Casalongue, H. S.; Vinh, D.; Dai, H. Ultrasmall reduced graphene oxide with high near-infrared absorbance for photothermal therapy. *J. Am. Chem. Soc.* **2011,** *133,* 6825-6831.

(54) Zhang, Y. J.; Shen, Y. F.; Yuan, J. H.; Han, D. X.; Wang, Z. J.; Zhang, Q. X.; Niu, L. Design and synthesis of multifunctional materials based on an ionic-liquid backbone. *Angew. Chem. Int. Edit.* **2006,** *45,* 5867-5870.

(55) Yang, S. L.; Xu, B. F.; Zhang, J. Q.; Huang, X. D.; Ye, J.; Yu, C. Z. Controllable Adsorption of Reduced Graphene Oxide onto Self-Assembled Alkanethiol Monolayers on Gold Electrodes: Tunable Electrode Dimension and Potential Electrochemical Applications. *J. Phys. Chem. C* **2010,** *114,* 4389-4393.

For TOC only